SUPPLEMENTAL FIGURES

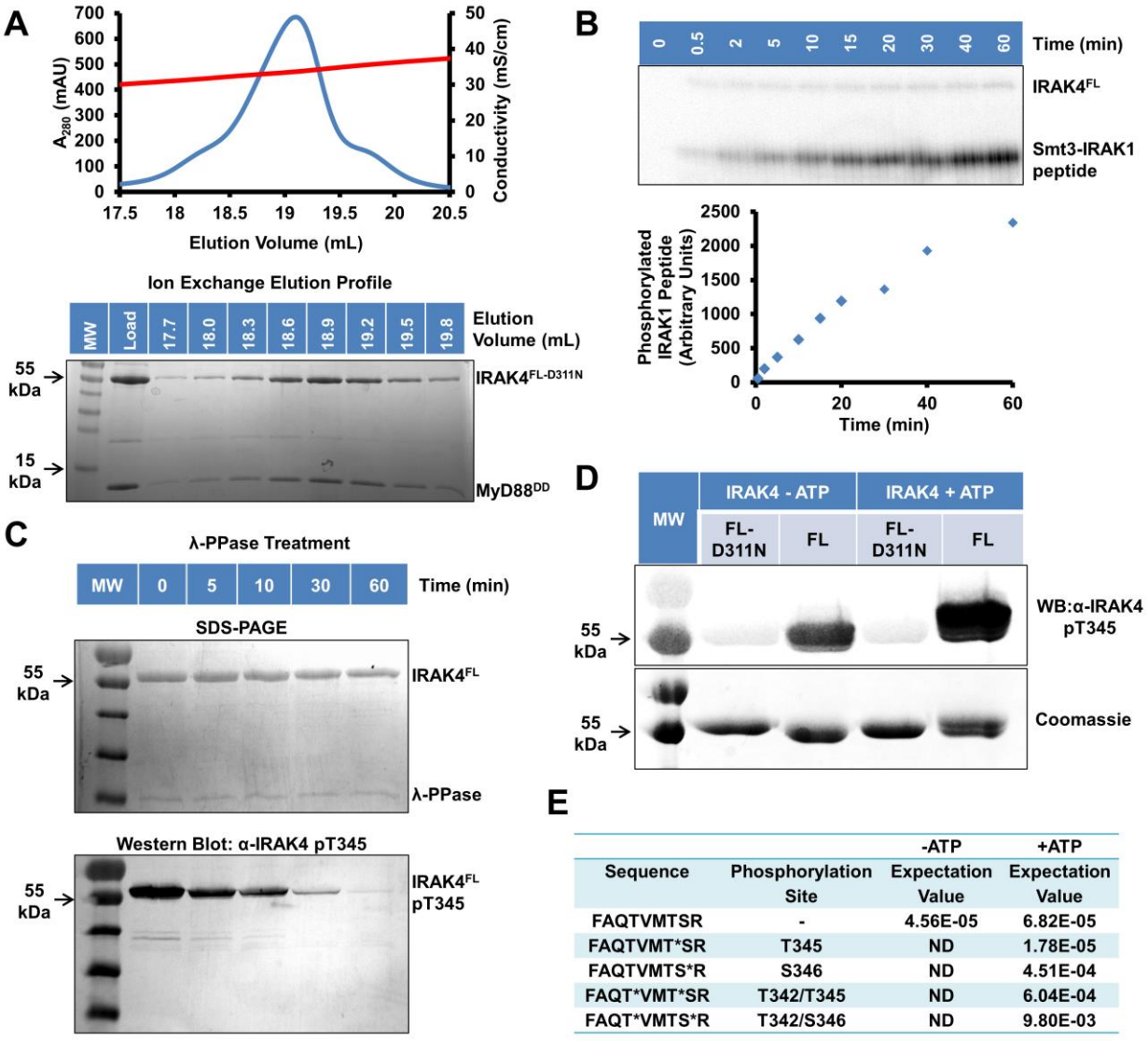

E

Sequence	Phosphorylation Site	-ATP Expectation Value	+ATP Expectation Value
FAQTVMTSR	-	4.56E-05	6.82E-05
FAQTVMT*SR	T345	ND	1.78E-05
FAQTVMTS*R	S346	ND	4.51E-04
FAQT*VMT*SR	T342/T345	ND	6.04E-04
FAQT*VMTS*R	T342/S346	ND	9.80E-03

Figure S1. Characterization of IRAK4 Activity and Phosphorylation State, Related to Figure 1

(A) Anion-exchange chromatography of co-expressed IRAK4$^{FL\text{-}D311N}$/MyD88^{DD} complex. A_{280} absorption profile (blue) shows major elution peak at a conductivity of approximately 35 mS/cm (red). SDS-PAGE of anion-exchange fractions followed by Coomassie blue staining indicates that the peak contains both IRAK4$^{FL\text{-}D311N}$ and MyD88^{DD}.

(B) Phosphorylation of 160 μM Smt3 tagged IRAK1 activation loop peptide (362-380) by 300 nM IRAK4^{FL}. Samples at various time points were separated by SDS-PAGE, visualized by autoradiography (top) and quantified (bottom).

(C) Dephosphorylation of IRAK4^{FL}. Natively phosphorylated IRAK4^{FL} was incubated with λ-phosphatase at 30 °C. Samples at various time points were analyzed by SDS-PAGE

followed by either Coomassie blue staining (top) or Western blot using a phospho-specific antibody for IRAK4 pT345 (bottom).

(D) Phosphorylation of insect cell purified $IRAK4^{FL}$ and $IRAK4^{FL\text{-}D311N}$ examined before and after incubation with 5 mM ATP at 25 °C. Samples were separated by SDS-PAGE and visualized by anti-IRAK4 pT345 Western blot (top) and Coomassie blue staining (bottom).

(E) Liquid Chromatography Tandem Mass Spectrometry (LC-MS/MS) of λ-phosphatase treated $IRAK4^{FL}$, with and without incubation with ATP/Mg^{2+}. Shown are the significant phosphorylation events on the IRAK4 activation loop residues, T342, T345, and S346, along with the expectation value of each ion.

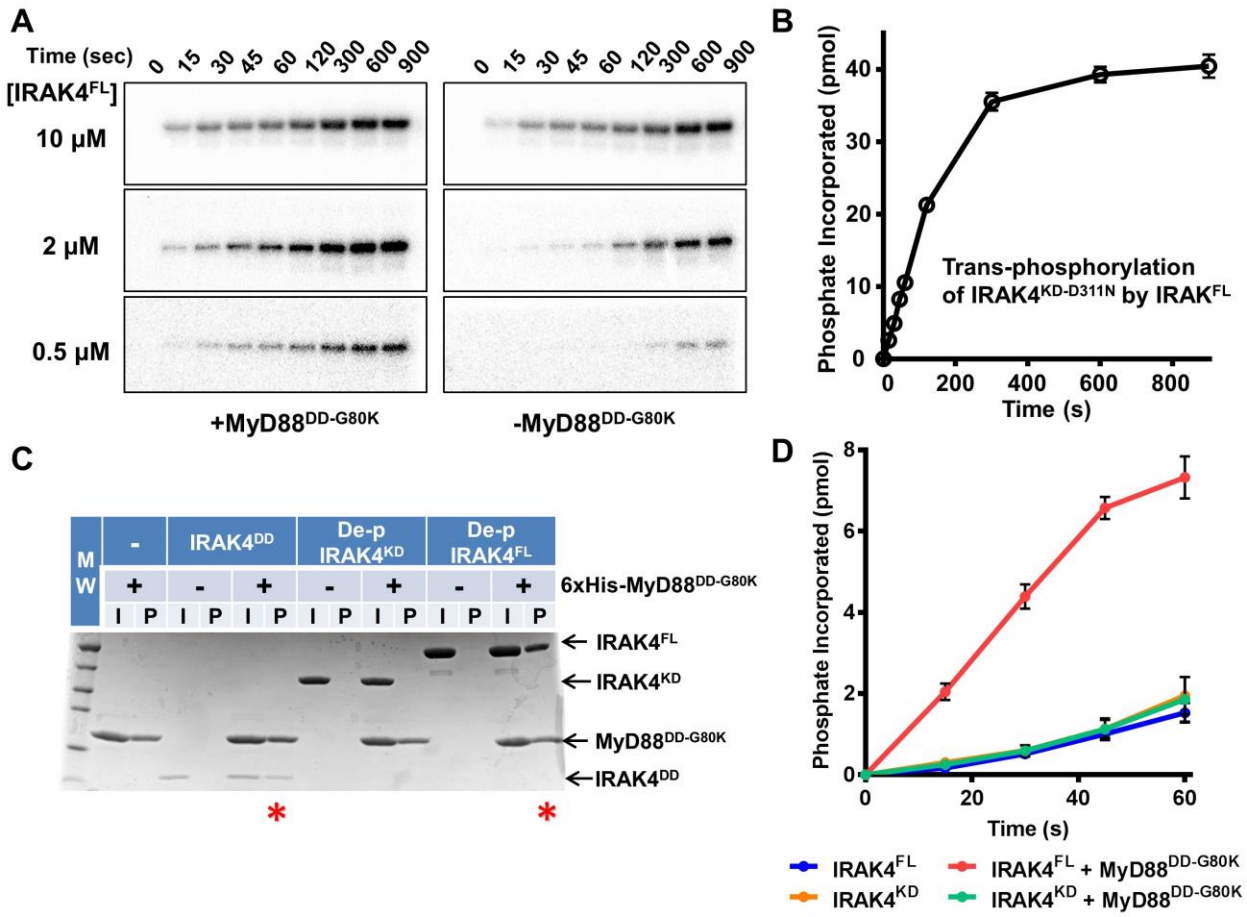

Figure S2. MyD88 Enhances *Trans*-autophosphorylation of IRAK4, Related to Figure 2

(A) Representative autoradiography images of $IRAK4^{FL}$ autophosphorylation with and without $MyD88^{DD\text{-}G80K}$. $IRAK4^{FL}$ samples at indicated concentrations were incubated with [γ-^{32}P]ATP and Mg^{2+} at 25 °C. $IRAK4^{FL}$ was pre-incubated with or without $MyD88^{DD\text{-}G80K}$. Timepoints were subjected to SDS-PAGE and visualized by autoradiography.

(B) *Trans*-phosphorylation of $IRAK4^{KD\text{-}D311N}$ (10 μM) by $IRAK4^{FL}$ (1 μM). The same data is shown as part of Figure 4F. Data represent mean ± SEM.

(C) Pull-down assay of 100 μM 6xHis tagged $MyD88^{DD\text{-}G80K}$ with 25 μM dephosphorylated $IRAK4^{DD}$, $IRAK4^{KD}$, or $IRAK4^{FL}$. Red asterisks indicate successful pull-down of IRAK4 construct. I: input, P: pulldown.

(D) Autophosphorylation of 2 μM dephosphorylated $IRAK4^{FL}$ or $IRAK4^{KD}$ with and without 50 μM $MyD88^{DD\text{-}G80K}$ preincubation. Data represent mean ± SEM.

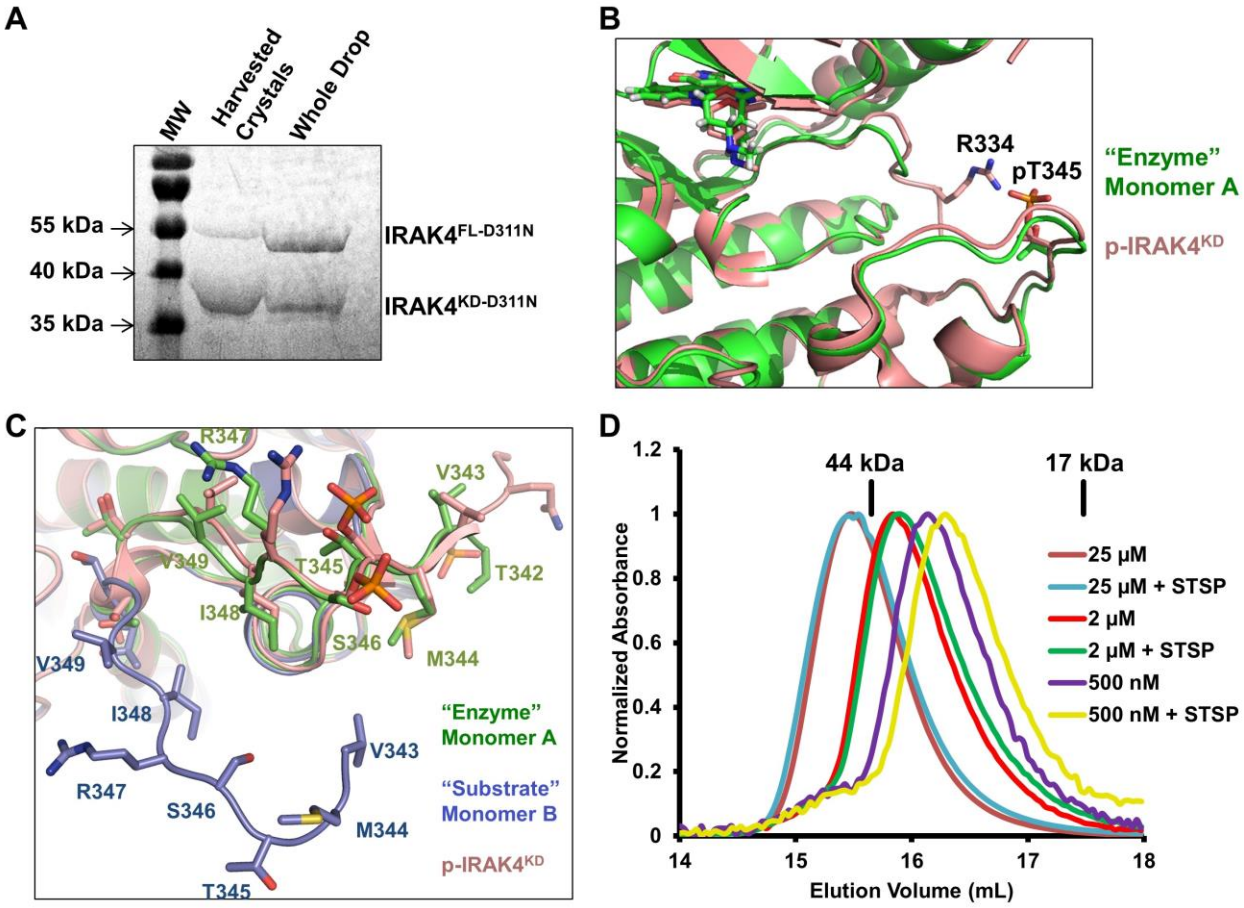

Figure S3. Activation Loop of Each IRAK4 Monomer Adopts a Distinct Conformation, Related to Figure 3

(A) Coomassie stained SDS-PAGE of IRAK4$^{FL\text{-}D311N}$ crystals and the crystallization drop. Several crystals were harvested and washed with reservoir solution before addition of SDS-PAGE loading buffer (Harvested Crystals). This was compared to the protein composition of the complete drop (Whole Drop), indicating that the crystals are enriched for the IRAK4 degradation product that is consistent in molecular weight with the IRAK4 kinase domain.

(B) Superposition of IRAK4$^{KD\text{-}D311N}$ "enzyme" monomer A with p-IRAK4^{KD} as in Figure 3B. The canonical phosphorylated residue, pT345 of p-IRAK4^{KD} and T345 of IRAK4$^{KD\text{-}D311N}$ are shown as sticks. R334 of p-IRAK4^{KD} forms a salt bridge with the phosphate group of pT345, but is disordered in the structure of IRAK4$^{KD\text{-}D311N}$.

(C) Superposition of IRAK4$^{KD\text{-}D311N}$ "enzyme" monomer A, "substrate" monomer B, and p-IRAK4^{KD}. The activation loop conformation of IRAK4$^{KD\text{-}D311N}$ "substrate" monomer B is distinct from that of IRAK4$^{KD\text{-}D311N}$ "enzyme" monomer A and p-IRAK4^{KD}. Activation loop residue side chains are shown as sticks and labeled for the IRAK4$^{FL\text{-}D311N}$ structure.

(D) Normalized size-exclusion chromatograms of IRAK4$^{KD\text{-}D311N}$ at indicated concentrations incubated with either DMSO or 500 µM staurosporine.

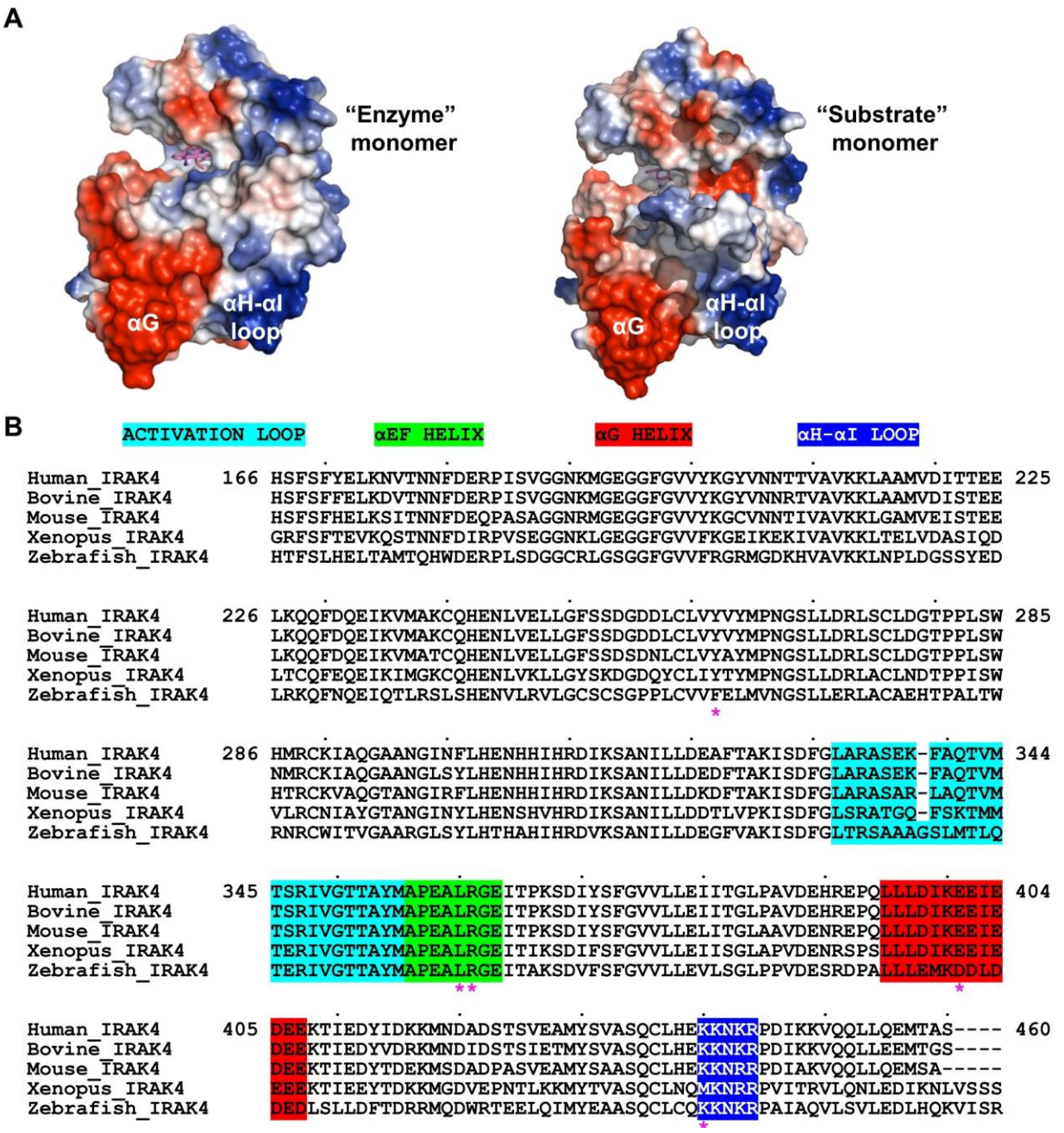

Figure S4. Residues at IRAK4 Dimer Interface are Highly Conserved, Related to Figure 4

(A) Surface electrostatics of αG and αH-I exo-sites at the IRAK4$^{KD\text{-}D311N}$ dimer interface. The interfaces are composed of highly negatively charged αG helix and highly positively charged αH-αI loop. In the dimer, each surface is juxtaposed with the complimentary surface of its partner.

(B) Alignment of IRAK4^{KD} orthologs from various species. Surfaces involved in IRAK4 dimerization, including the activation loop, αEF helix, αG helix, and αH-αI loop are highlighted in cyan, green, red and blue, respectively. Pink asterisks indicate sites of mutagenesis.

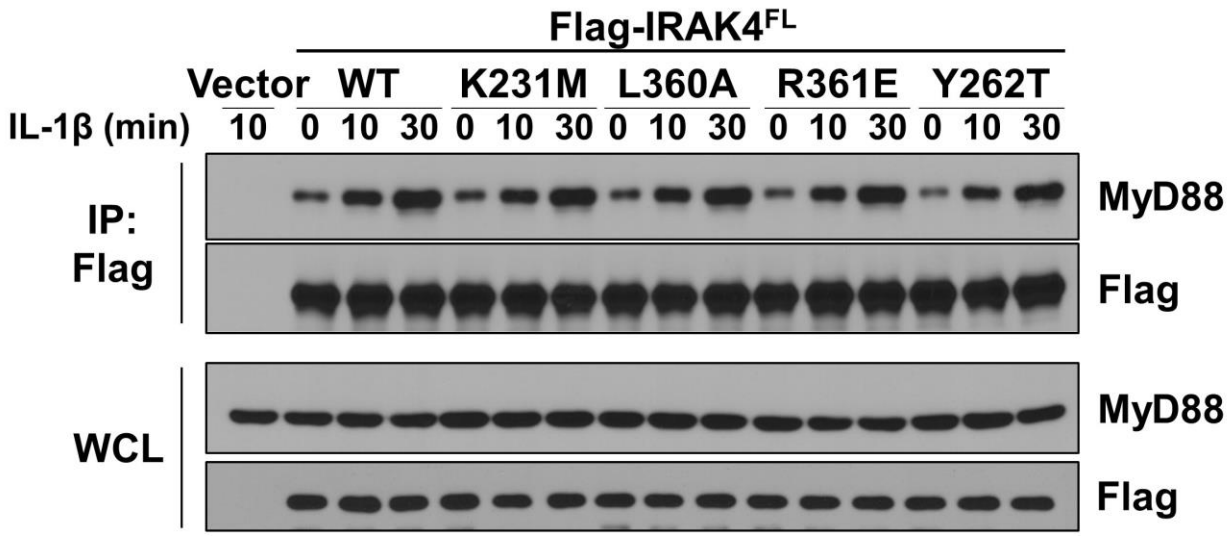

Figure S5. IRAK4 Kinase Domain Mutations do not Disrupt interaction with MyD88, Related to Figure 5

IRAK4-deficient human fibroblasts were infected with retroviruses containing empty vector construct (Vector), Flag-tagged IRAK4^{FL} wild-type (WT) and mutants (K213M, L360A, R361E, and Y262T). Cells were treated with IL-1β (1 ng/mL) for the indicated times, followed by immunoprecipitation (IP) with Flag antibody and Western blot for MyD88. Western blot of whole cell lysate (WCL) was included to control for MyD88 and Flag-IRAK4 expression levels.

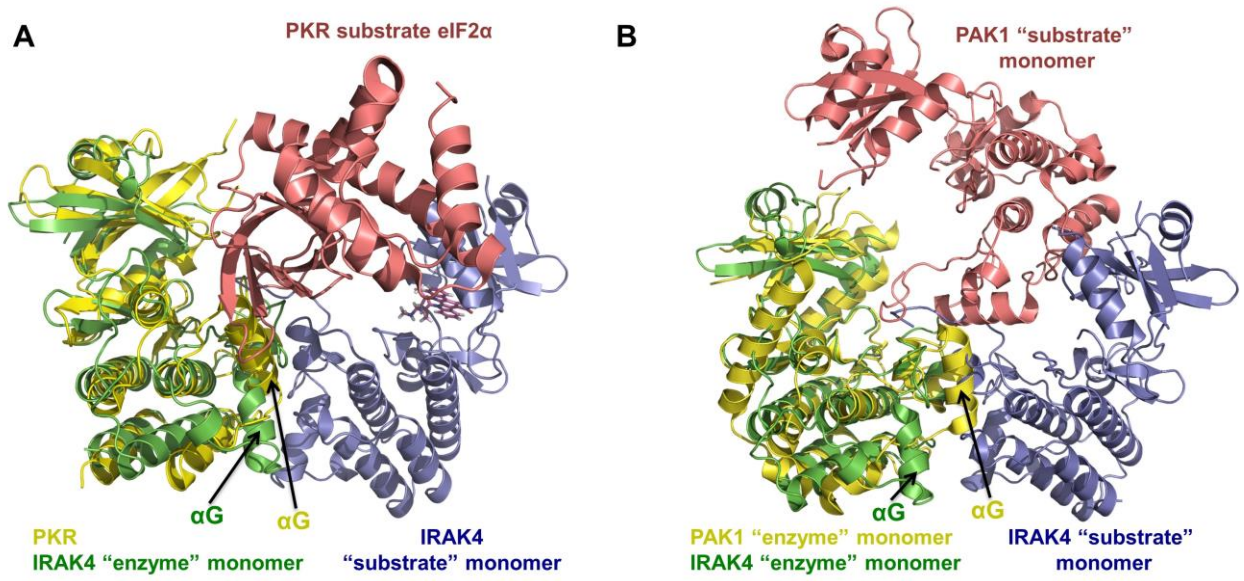

Figure S6. Comparison of the IRAK4 Asymmetric Enzyme-Substrate Dimer with PKR and PAK1, Related to Figure 7

(A) The KD of PKR (yellow) is superimposed with the IRAK4$^{KD\text{-}D311N}$ "enzyme" monomer. The PKR substrate eIF2α also interacts with the PKR αG helix. Similarly, the IRAK4 "substrate" monomer interacts with the IRAK4 "enzyme" monomer αG helix.

(B) The "enzyme" monomers of PAK1 (yellow) and IRAK4$^{KD\text{-}D311N}$ (green) are superimposed. The "substrate" monomers of PAK1 (pink) and IRAK4$^{KD\text{-}D311N}$ (blue) are in distinct locations, illustrating the large differences between the dimerization interfaces.

SUPPLEMENTAL EXPERIMENTAL PROCEDURES

Cloning and Protein Purification

PCR fragments of human IRAK4, FL (1-460) and KD (154-460), were inserted into pFastBacHTB between BamHI and NotI restriction sites. Plasmids were transformed into DH10Bac™ *E. coli* competent cells followed by bacmid purification using the Bac-to-Bac® baculoviral expression system. Bacmids were transfected into Sf9 monolayer cells to generate baculoviruses. Harvested baculoviruses were used to infect High Five™ cells for 48 hours at 27 °C. Cells were harvested by centrifugation and resuspended in lysis buffer containing 50 mM Hepes-NaOH at pH 7.5, 300 mM NaCl, 10 mM imidazole and 1mM TCEP-HCl. DNase (10 µg/mL) and protease inhibitors (SIGMAFAST™ Protease Inhibitor Cocktail Tablets, EDTA-Free) were added to the lysate. Cells were lysed with an Avestin EmulsiFlex-*C3* homogenizer. Cell debris was cleared via centrifugation at 48,400 relative centrifugal force (RCF). Clarified lysates were incubated with HisPur™ Cobalt Resin and washed extensively with lysis buffer. Bound proteins were eluted with lysis buffer supplemented with 150 mM imidazole. The eluates were immediately further purified with anion exchange chromatography using Source 15Q resin, followed by N-terminal 6xHis-tag cleavage using overnight incubation with 6xHis-TEV at 4 °C. When desired, IRAK4 was dephosphorylated via the simultaneous addition of 6xHis-λ-phosphatase and 5 mM $MnCl_2$. Removal of TEV and λ-phosphatase was facilitated with HisPur™ Cobalt Resin and anion exchange. IRAK4 was then further purified with a final size-exclusion chromatography (SEC) step in 20 mM Hepes-NaOH at pH 7.5, 150 mM NaCl and 1mM TCEP-HCl. Fractions containing IRAK4 were pooled, concentrated, and flash frozen in liquid N_2. To generate phosphorylated $IRAK4^{FL}$ and $IRAK4^{KD}$, the proteins were incubated with 5 mM ATP and 10 mM $MgCl_2$ for 1 hour at 25 °C. Coexpression of His-$IRAK4^{FL\text{-}D311N}$ and $MyD88^{DD}$ (20-124) was achieved by insertion into pFastBacDual. Generation of bacmid, expression, and purification were performed as detailed above.

DNA containing MyD88 (20-154) and IRAK4 (4-106) was obtained by PCR and inserted into pET26 between NdeI and NotI restriction sites. The MyD88 G80K mutation and all IRAK4 mutations were introduced using the QuikChange II Site-Directed Mutagenesis Kit (Agilent Technologies). Plasmids were transformed into *E. coli* BL21-CodonPlus® (DE3)-RIPL competent cells. Cells were grown to an OD_{600} of 0.6, followed by induction with 0.4 mM IPTG and overnight incubation at 20 °C. Cells were resuspended, lysed, and clarified as detailed above, without the addition of DNase or protease inhibitors. $MyD88^{DD}$ (20-154), $MyD88^{DD\text{-}G80K}$ (20-154), and IRAK4 (4-106) were then purified with HisPur™ Cobalt Resin followed by size-exclusion chromatography as detailed above.

Multi-Angle Light Scattering (MALS)

For molecular mass determination by MALS, protein samples were injected into a Superdex 200 (10/300 GL) gel filtration column (GE Healthcare) equilibrated with SEC buffer (above). The chromatography system was coupled to a three-angle light scattering detector (mini-DAWN TRISTAR) and a refractive index detector (Optilab DSP) (Wyatt Technology). Data were collected every 0.5 s with a flow rate of 0.5 mL/min. Data analysis was carried out using ASTRA V.

Sedimentation Equilibrium Analytical Ultracentrifugation (SE-AUC)

Experiments were performed in a Beckman Coulter Optima XL-A ultracentrifuge with an An-60 Ti rotor using six-channel centerpieces and quartz glass. Following SEC, $IRAK4^{FL\text{-}D311N}$ was

diluted with SEC buffer to final concentrations of 6.4 μM, 4.8 μM, and 2.9 μM. Absorbance at 280 nm was collected, with SEC buffer serving as the blank. Samples were run at 4 °C. Sedimentation equilibrium was attained at speeds of 12,000 RPM, 15,000 RPM, 18,000 RPM, 22,000 RPM and 31,000 RPM. Data was processed with the programs Sedfit and Sedphat (Schuck, 2003) using a monomer-dimer self-association model. Buffer density and partial specific volume were calculated using the program Sednterp (Laue et al., 1992).

Crystallization, Data Collection and Structure Determination

$IRAK4^{KD\text{-}D311N}$ at 10 mg/mL was incubated with staurosporine at a 2:1 molar ratio prior to setting up crystallization trays. Crystals were obtained by hanging drop vapor diffusion at 16-20 °C by mixing equal volumes of protein and reservoir solution (1.6-1.9 M ammonium sulfate, 100 mM Hepes-NaOH at pH7). Crystals were harvested, cryoprotected with reservoir solution supplemented with 20 % (v/v) ethylene glycol, and flash frozen in liquid nitrogen. Native data collection was performed at Brookhaven National Laboratory using the National Synchrotron Light Source (NSLS) beamline X29, while sulfur anomalous data was collected at NSLS beamline X4A. Data reduction was accomplished with XDS/XSCALE (Kabsch, 2010), followed by Ellipsoidal Truncation and Anisotropic Scaling (Strong et al., 2006) and solved by molecular replacement using Phenix (Adams et al., 2010). Model building and refinement were done with coot (Emsley and Cowtan, 2004) and Phenix (Adams et al., 2010). Figures were generated using Pymol (Delano, 2002). The final atomic model contains residues H166-L215, L226-S252, L258-A333 and T342-T458 in the “enzyme” monomer (A), and H166-A217, L226-D254, L258-F330 and V343-T458 in the “substrate” monomer (B).

Kinase Assays

Purified dephosphorylated IRAK4 was subjected to autophosphorylation and *trans*-phosphorylation experiments using [γ-^{32}P]ATP. IRAK4 samples at various concentrations were pre-incubated with or without 50 μM MyD88 G80K in kinase assay buffer containing 20 mM Hepes-NaOH pH 7.5, 150 mM NaCl, 1 mM TCEP, 10 mM $MgCl_2$, 50 mM Sodium Fluoride and 20 mM β-glycerophosphate for 30 minutes at 25 °C. Reactions were started by the addition of 5 mM [γ-^{32}P]ATP and incubated at 25 °C. At different time points, reactions were quenched by the addition of SDS-PAGE loading buffer containing 100 mM EDTA. Phosphoproteins were separated from free nucleotides on 12 % SDS-PAGE gels and visualized by autoradiography using a Fuji BAS-2500 apparatus. Incorporated phosphate was quantified by comparison to [γ-^{32}P]ATP dilution series using Image Gauge (FUJIFILM) software.

Biological Reagents and Cell Culture

Recombinant human IL-1β was purchased from R&D system. Antibodies against IκBα, MyD88, Mouse Anti-rabbit IgG (Conformation Specific) and phosphorylated IκBα (Ser32/S36), JNK and IKKα/β (Ser176/180) were purchased from Cell signaling. Antibodies to Flag (anti-Flag) and to actin were purchased from Sigma and Santa Cruz Biotechnologies, respectively. HEK293/IL-1RI cells and human IRAK4-deficient fibroblasts were maintained in Dulbecco's modified Eagle's medium, supplemented with 10 % fetal bovine serum, penicillin G (100 μg/mL) and streptomycin (100 μg/mL).

Plasmids and Retroviruses

Human IRAK4 cDNA was purchased from Open Biosystems. The IRAK4 mutants were generated by site-directed mutagenesis polymerase chain reaction. The WT and mutants of IRAK4 were cloned into pMXs-IRES-Puro retroviral expression vector and transfected into

phoenix cells for viral packaging. Human IRAK4-deficient fibroblasts were infected by the packaged retrovirus for 3 days and selected by puromycin (2 μg/mL) for 2 days for stable viral integration. For all PCR reactions high fidelity Pfu Turbo polymerase was used (Stratagene).

Immunoblotting and Co-immunoprecipitation

Cells were harvested and lysed in a Triton-containing lysis buffer (0.5% Triton X-100, 20 mM HEPES (pH 7.4), 150 mM NaCl, 12.5 mM β-glycerophosphate, 1.5 mM $MgCl_2$, 10 mM NaF, 2 mM dithiothreitol, 1 mM sodium orthovanadate, 2mM EGTA, 1 mM phenylmethylsulfonyl fluoride and complete protease inhibitor cocktail from Roche). Cell lysates were then separated by 10% SDS-PAGE, transferred to Immobilon-P membranes (Millipore), and subjected to immunoblotting. For co-immunoprecipitations, cell lysates were incubated with 20 μL of protein A-Sepharose beads with anti-Flag antibody at 4 °C overnight, and beads were washed with 1 mL of lysis buffer 5 times before being dissolved in 40 μL of Laemmli buffer.

Quantitative Real-Time PCR

Total RNA was isolated using TRIzol reagent (Invitrogen). 3 μg of total RNA was then used for reverse transcription reaction using SuperScript-reverse transcriptase (Invitrogen). Quantitative PCR was performed in AB 7300 RealTime PCR System, and the gene expression of human IL-8, TNFα, and actin was examined by SYBR® GREEN PCR Master Mix (Applied Biosystems). PCR amplification was performed in triplicate, and water was used to replace cDNA in each run as a negative control. The reaction protocol included pre-incubation at 95°C to activate FastStart DNA polymerase for 10 min, amplification of 40 cycles that was set for 15 s at 95 °C, and annealing for 60 s at 60 °C. The results were normalized with the housekeeping gene β-actin. Primer sequences were designed using AlleleID 6.0. The following primers were used: human IL-8 forward, AGAGACAGCAGAGCACAC; human IL-8 reverse, GTTCTTTAGCACTCCTTGGC; human TNFα forward, TCAGCAAGGACAGCAGAG; human TNFα reverse, GTATGTGAGAGGAAGAGAACC; human actin forward, GTCGGTATGGGTCAGAAAG; human actin reverse, CTCGTTGTAGAAGGTGTGG.

Small- and Wide-Angle X-Ray Scattering (SAXS/WAXS)

To remove any aggregates and to ensure conformational homogeneity, the $IRAK4^{FL\text{-}D311N}$/$MyD88^{DD}$ complex was purified with SEC immediately prior to SAXS. Data was collected at concentrations of 2, 1, and 0.5 mg/mL. Both small- and wide-angle X-ray scattering (SAXS/WAXS) data were collected in triplicate at NSLS X9 with an incident wavelength of 0.92 Å. SAXS and WAXS data merging, radial averaging, and buffer subtraction was performed with pyXS. Scaling and merging of data from different concentrations and Guinier analysis were performed with Primus (Konarev et al., 2003). Evaluation of the particle distance distribution function P(r) was accomplished with GNOM (Svergun, 1991) using a maximum linear dimension D_{max} of 212.5 Å. *Ab initio* modeling was performed with DAMMIF (Franke and Svergun, 2009). Twenty independent DAMMIF models were further processed with DAMAVER (Volkov and Svergun, 2003). The mean normalized spatial discrepancy (NSD) of the 20 independent models was 1.118 with a standard deviation (SD) of 0.110. One model was discarded due to an NSD greater than the mean + 2SD. The remaining 19 models were aligned, averaged, and filtered. Structures of the binary MyD88/IRAK4 DD complex (PDB: 3MOP) and IRAK4 KD dimers were placed into the resulting filtered volume. We then calculated the scattering profile of our fitted model using the program CRYSOL (Svergun et al., 1995) and fit it to the experimental scattering data.

Molecular Dynamics Simulations

Simulation systems were set up by placing the IRAK4 kinase dimer in a cubic simulation box (with periodic boundary conditions) of at least 97 Å per side and approximately 85,000 atoms in total. Explicitly represented water molecules were added to fill the system, and Na^+ and Cl^- ions were added to maintain physiological salinity (150 mM) and to obtain a neutral total charge for the system. The systems were parameterized using the CHARMM36 force field with TIP3P water (Best et al., 2012; Jorgensen et al., 1983; MacKerell et al., 1998) and then equilibrated in the NPT ensemble at 1 bar and 310 K for 10 ns. Equilibrium molecular dynamics simulations were performed on the special-purpose molecular dynamics machine Anton in the NVT ensemble at 310 K using the Nose-Hoover thermostat (Hoover, 1985) with a relaxation time of 1.0 ps and a time step of 2.5 fs. All bond lengths to hydrogen atoms were constrained using a recently developed implementation (Lippert et al., 2007) of M-SHAKE (Kräutler et al., 2001). The Lennard-Jones and the Coulomb interactions in the simulations were calculated using a force-shifted cutoff of 12 Å (Beck et al., 2005).

SUPPLEMENTAL REFERENCES

Adams, P.D., Afonine, P.V., Bunkoczi, G., Chen, V.B., Davis, I.W., Echols, N., Headd, J.J., Hung, L.W., Kapral, G.J., Grosse-Kunstleve, R.W.*, et al.* (2010). PHENIX: a comprehensive Python-based system for macromolecular structure solution. Acta Crystallogr D Biol Crystallogr *66*, 213-221.

Beck, D.A., Armen, R.S., and Daggett, V. (2005). Cutoff size need not strongly influence molecular dynamics results for solvated polypeptides. Biochemistry *44*, 609-616.

Best, R.B., Zhu, X., Shim, J., Lopes, P.E., Mittal, J., Feig, M., and Mackerell, A.D., Jr. (2012). Optimization of the additive CHARMM all-atom protein force field targeting improved sampling of the backbone phi, psi and side-chain chi(1) and chi(2) dihedral angles. Journal of chemical theory and computation *8*, 3257-3273.

Delano, W.L. (2002). The PyMol Molecular Graphics System.

Emsley, P., and Cowtan, K. (2004). Coot: model-building tools for molecular graphics. Acta Crystallogr D Biol Crystallogr *60*, 2126-2132.

Franke, D., and Svergun, D.I. (2009). DAMMIF, a program for rapid ab-initio shape determination in small-angle scattering. Journal of Applied Crystallography *42*, 342-346.

Hoover, W.G. (1985). Canonical dynamics: Equilibrium phase-space distributions. Physical Review A *31*, 1695-1697.

Jorgensen, W.L., Chandrasekhar, J., Madura, J.D., Impey, R.W., and Klein, M.L. (1983). Comparison of simple potential functions for simulating liquid water. The Journal of chemical physics *79*, 926-935.

Kabsch, W. (2010). Xds. Acta Crystallogr D Biol Crystallogr *66*, 125-132.

Konarev, P.V., Volkov, V.V., Sokolova, A.V., M.H.J., K., and Svergun, D.I. (2003). PRIMUS: a Windows PC-based system for small-angle scattering data analysis. J. Appl. Cryst. *36*, 1277-1282.

Kräutler, V., van Gunsteren, W.F., and Hünenberger, P.H. (2001). A fast SHAKE algorithm to solve distance constraint equations for small molecules in molecular dynamics simulations. Journal of Computational Chemistry *22*, 501-508.

Laue, T.M., Shah, B.D., Ridgeway, T.M., and Pelletier, S.L. (1992). Computer-aided interpretation of analytical sedimentation data for proteins. In Analytical Ultracentrifugation in Biochemistry and Polymer Science, S.E. Harding, A.J. Rowe, and J.C. Horton, eds. (Cambridge, UK: Royal Society of Chemistry), pp. 90–125.

Lippert, R.A., Bowers, K.J., Dror, R.O., Eastwood, M.P., Gregersen, B.A., Klepeis, J.L., Kolossvary, I., and Shaw, D.E. (2007). A common, avoidable source of error in molecular dynamics integrators. The Journal of chemical physics *126*, -.

MacKerell, A.D., Bashford, D., Bellott, Dunbrack, R.L., Evanseck, J.D., Field, M.J., Fischer, S., Gao, J., Guo, H., Ha, S.*, et al.* (1998). All-Atom Empirical Potential for Molecular Modeling and Dynamics Studies of Proteins†. The Journal of Physical Chemistry B *102*, 3586-3616.
Schuck, P. (2003). On the analysis of protein self-association by sedimentation velocity analytical ultracentrifugation. Analytical biochemistry *320*, 104-124.
Strong, M., Sawaya, M.R., Wang, S., Phillips, M., Cascio, D., and Eisenberg, D. (2006). Toward the structural genomics of complexes: crystal structure of a PE/PPE protein complex from Mycobacterium tuberculosis. Proceedings of the National Academy of Sciences of the United States of America *103*, 8060-8065.
Svergun, D. (1991). Mathematical methods in small-angle scattering data analysis. J Appl Cryst *24*, 485-492.
Svergun, D., Baraberato, C., and Koch, M.H. (1995). CRYSOL - a Program to evaluate X-ray Solution Scattering of Biological Macromolecules from Atomic Coordinates. J. Appl. Cryst. *28*, 768-773.
Volkov, V.V., and Svergun, D.I. (2003). Uniqueness of ab initio shape determination in small-angle scattering. Journal of Applied Crystallography *36*, 860-864.